NON-CHAOS-MEDIATED MIXED-MODE OSCILLATIONS IN AN EXTENDED HINDMARSH-ROSE NEURONAL OSCILLATOR WITH TIME DELAY

by

Jiangang ZHANG*, Lixiang WEI, Xinlei AN, and Mengran NAN

School of Mathematics and Physics, Lanzhou Jiaotong University, Lanzhou, Gansu, China

Original scientific paper
https://doi.org/10.2298/TSCI2203427Z

This paper proposes an extended neuron model with time delay. It aims to investigate the effect of time delay on the dynamical behavior of the system under different conditions. The existence of the Hopf bifurcation of the system and the stability of its periodic solution are proved by the central manifold theorem. Numerical results show that the system has abundant dynamical performance, including chaos, period-adding, and intermittent chaos.

Key words: *time delay, Hopf bifurcation, mixed-mode oscillations, two-parameter characteristics*

Introduction

The chaos theory describes how a slight change in the starting conditions of a system can dramatically affect how it develops. Chaos is usually considered a large-scale phenomenon associated with classical physics, and does not exist in the microscopic quantum realm. At any a given time, a dynamical system has a set of states given by a set of real numbers, which can be represented by a point in the appropriate state space. In recent years, the study of the dynamics of chaotic systems in 2-D parametric space has made great progress in theory and practical applications [1, 2]. Junges and Gallas [3] reported high-resolution stability diagrams for wide ranges of the main control parameters of the laser described by the Lang-Kobayashi model. In particular, they discussed the parameter influence on dynamical performance and mapped the distribution of chaotic pulsations and self-generated periodic spiking with arbitrary periodicity.

The mixed-mode oscillations consist of periodic cycles having a number of large peaks intercalated by a number of small peaks in one period of the oscillation. In general, the chemical oscillations always appear as mixed-mode oscillations, a complex dynamical behavior observed abundantly both numerically and experimentally in numerous prototypical systems. In biological systems, mixed-mode oscillations have potential relevance for signal encoding [4]. The mixed-mode oscillations are typically encountered in parameter domains where the dynamics change from periodic to chaotic oscillations. The mixed-mode oscillations have also been observed in a wide variety of oscillating chemical systems [5], and there are many recent reviews about mixed-mode oscillations and their applications [6-9].

* Corresponding author, e-mail: zhangjg7715776@126.com

In this paper, we mainly focused on the following extended Hindmarsh-Rose neuronal oscillator [8]:

$$\begin{aligned} \dot{x} &= ay + bx^2 - cx^3 - dz + I_{DC} \\ \dot{y} &= e - fx^2 - y - gw \\ \dot{z} &= \mu\left[-z + s\left(x + h\right)\right] \\ \dot{w} &= v\left[-kw + r\left(y + l\right)\right] \end{aligned} \tag{1}$$

where the constants *a, b, c, d, e, f, g, μ, s, h, v, k, r,* and *l* express the current and conductance based dynamical parameters, I_{DC} – the injected current, x – the membrane voltage, y – a fast current, z – a slow current since $\mu \ll 1$, w – a slow dynamical process as $v < \mu \ll 1$, μ – the ratio of time scales between fast and slow fluxes across the membrane of neuron, and v controls the speed of variation of the slower dynamical process w, particularly the calcium exchange between intracellular warehouse and the cytoplasm. Since the oscillation of the slow subsystem drives the dynamical behavior of the fast subsystem, there is a time delay in the process. Therefore, the time delay needs to be considered. The following system was established:

$$\begin{aligned} \dot{x} &= ay + bx^2 - cx^3 - dz + I_{DC} \\ \dot{y} &= e - fx^2 - y - gw\left(t - \tau\right) \\ \dot{z} &= \mu\left[-z + s\left(x + h\right)\right] \\ \dot{w} &= v\left[-kw + r\left(y + l\right)\right] \end{aligned} \tag{2}$$

The system can be solved analytically by the multiple scales method [10], frequency analysis [11-14], He-Laplace method [15], the variational principle [16-20], the homotopy perturbation [21, 22], Fourier spectral method [23], and direct algebraic method [24]. For numerical simulation, He-Li's neural network computation is recommended for its high simulation efficiency [25]. However, the chaotic properties of eq. (2) cannot be fully revealed by the above methods, and this paper will apply the central manifold theorem for this purpose.

The stability of equilibrium point and existence analysis of Hopf bifurcation

In this section, we focus on the system's stability at the point of equilibrium and the existence of Hopf bifurcation.

Make the equilibrium point $E_* = (x_*, y_*, z_*, w_*)$, let $\bar{x}(t) = x(t) - x_*$, $\bar{y}(t) = y(t) - y_*$, $\bar{z}(t) = z(t) - z_*$, $\bar{w}(t) = w(t) - w_*$, and still note $\bar{x}(t), \bar{y}(t), \bar{z}(t)$, and $\bar{w}(t)$ by $x(t)$, $y(t)$, $z(t)$, and $w(t)$. Then the Jacobi matrix corresponding to the system (2) at the origin is:

$$J = \begin{bmatrix} 2bx_* - 3cx_*^2 & a & -d & 0 \\ -2fx_* & -1 & 0 & -ge^{-\lambda\tau} \\ \mu s & 0 & -\mu & 0 \\ 0 & vr & 0 & -kv \end{bmatrix}$$

So the corresponding characteristic equation of the system (2) at the origin is:

$$F(\lambda)=\lambda^4+m_3\lambda^3+m_2\lambda^2+m_1\lambda+m_0+(n_2\lambda+n_1\lambda+n_0)\mathrm{e}^{-\lambda\tau} \tag{3}$$

where

$$m_3=3cx_*^2-2bx_*+kv+\mu+1$$

$$m_2=3cx_*^2-2bx_*+(3cx_*^2-2bx_*+1)\mu+(3cx_*^2-2bx_*+1+\mu)kv+\mu sd$$

$$m_1=(3cx_*^2-2bx_*)\mu+[3cx_*^2-2bx_*+(3cx_*^2-2bx_*+1)\mu]kv+dkv\mu s+\mu sd$$

$$m_0=(3cx_*^2-2bx_*)\mu kv+dkv\mu s$$

$$n_2=vrg,\quad n_1=(3cx_*^2-2bx_*+1)vrg,\quad n_0=(3cx_*^2-2bx_*)\mu vrg+dg\mu svr$$

Then τ is divided into two cases for discussion.

Case 1: $\tau = 0$

Theorem 1. The equilibrium point $E_*=(x_*,y_*,z_*,w_*)$, is locally asymptotically stable when $\tau = 0$.

Proof. If $\tau = 0$, then eq. (3) can be reduced to:

$$\lambda^4+m_{11}\lambda^3+m_{12}\lambda^2+m_{13}\lambda+m_{14}=0 \tag{4}$$

where $m_{13}=m_3, m_{12}=m_2+n_2, m_{11}=m_{11}+n_{11}, m_{10}=m_0+n_0$. According to the Routh-Hurwitz criterion, the following result can be obtained: $m_{11}>0$, $m_{13}>0$, $m_{11}m_{12}m_{13}>m_{11}^2m_{14}+m_{13}^2$, then all roots of eq. (4) have negative real parts, and the system is locally asymptotically stable at the equilibrium point.

Case 2: $\tau > 0$

Theorem 2. The system (2) is asymptotically stable at the equilibrium point $E_*=(x_*,y_*,z_*,w_*)$ when $\tau\in[0,\tau^*)$ and it is unstable when $\tau>\tau^*$.

Proof. Suppose that $\lambda = i\omega$ is a root of eq. (3), then we can have:

$$(n_0-n_2\omega^2)\cos\omega\tau+n_1\omega\sin\omega\tau=m_2\omega^2-\omega^4-m_0$$

$$(-n_0+n_2\omega^2)\sin\omega\tau+n_1\omega\cos\omega\tau=m_3\omega^3-m_1\omega$$

Let:

$$a\sin(\omega\tau)+b\cos(\omega\tau)=c,\quad a\cos(\omega\tau)-b\sin(\omega\tau)=d \tag{5}$$

where $a=n_1\omega, b=n_0-n_2\omega^2, c=m_2\omega^2-\omega^4-m_0,$ and $d=m_3\omega^3-m_1\omega.$

From this, it is easy to obtain:

$$a^2+b^2=c^2+d^2\Rightarrow\omega^8+C_3\omega^6+C_2\omega^4+C_1\omega^2+C_0=0 \tag{6}$$

where $C_3=m_3^2-2m_2,\quad C_2=m_2^2+2m_0-2m_1m_3-n_2^2,\quad C_1=m_1^2-2m_0m_2-n_1^2+2n_0n_2$, and $C_0=m_0^2-n_0^2$.

Let $v=\omega^2$, then eq. (3) will be transformed into:

$$v^4+C_3v^3+C_2v^2+C_1v+C_0=0 \tag{7}$$

If eq. (6) has a positive root v^*, then eq. (5) has a positive root $\omega=\sqrt{v^*}$. Then from eq. (5) we have:

$$\cos(\omega\tau^*)=\frac{bc+ad}{a^2+b^2}\Rightarrow\tau^*=\frac{1}{\omega}\left\{\arccos\left(\frac{bc+ad}{a^2+b^2}\right)\right\}$$

Theorem 3. For $\tau > 0$, it is easy to obtain that the system (2) is locally asymptotically stable at the equilibrium point $E_*=(x_*,y_*,z_*,w_*)$ when $\tau\in\tau[0,\tau^*)$; the system (4) undergoes a Hopf bifurcation at the equilibrium point $E_*=(x_*,y_*,z_*,w_*)$ when $\tau=\tau^*$, and from this $E_*=(x_*,y_*,z_*,w_*)$ can be obtained a set of periodic solutions.

Proof. Consider that H_1: eq. (7) has a positive root v_{10}. Then eq. (6) has a positive root $\omega_{10}=\sqrt{v_{10}}$. Eliminate $\sin(\omega\tau)$ from eq. (7) and replace ω with ω_{10}, we obtain:

$$\tau^*=\frac{1}{\omega_{10}}\left\{\arccos\left[\frac{N_1(\omega_{10})}{N_2(\omega_{10})}\right]\right\} \tag{8}$$

with

$$N_{21}(\omega_{20})=n_2\omega_{10}^6+(m_3n_1-m_2n_2)\omega_{10}^4+(m_0n_2-m_1n_1+m_2n_0)\omega_{10}^2+m_0n_0$$

$$N_{22}(\omega_{10})=n_2{}^2\omega_{10}^4+(n_1{}^2-2n_2n_0)\omega_{10}^2+n_0{}^2$$

From this, it is possible to obtain:

$$\mathrm{Re}\left[\frac{\mathrm{d}\lambda}{\mathrm{d}\tau_1}\right]^{-1}_{\lambda=i\omega_{10}}=\frac{m_1'(v_{10})}{N_{22}(\omega_{10}{}^2)} \tag{9}$$

Therefore:

$$\mathrm{Re}\left[\frac{\mathrm{d}\lambda}{\mathrm{d}\tau_1}\right]^{-1}_{\lambda=i\omega_{10}}\neq 0$$

if condition:

$$H_2: m_1'(v_{10})=\frac{\mathrm{d}m_1(v_{10})}{\mathrm{d}v_1}\Big|_{v_1=v_{10}}\neq 0$$

where $m_1(v_{10})=v_{10}{}^4+C_3v_{10}{}^3+C_2v_{10}{}^2+C_1v_{10}+C_0=0$. Thus, according to the H_1 H_2 we can prove the *Theorem 3*.

Local stability and direction of Hopf bifurcation

In the previous section, we discussed the stability around the equilibrium point and the existence of Hopf bifurcations based on the extended Hindmarsh-Rose neuron model. In this section, the stability and bifurcation direction of the Hopf bifurcation period solution will be further discussed.

Theorem 3 (the central manifold theorem).

- The μ_2 determines the direction of Hopf bifurcation: if $\mu_2 > 0$ and $\tau_k > \tau_0$, the system has a supercritical Hopf bifurcation near the equilibrium point; if $\mu_2 < 0$ and $\tau_k < \tau_0$, the system will have a subcritical Hopf bifurcation; there is a bifurcating periodic solution in the corresponding time delay.
- The T_2 determines the cycle of bifurcating periodic solutions: if $T_2 > 0$ ($T_2 < 0$), the period of periodic solution increases (decreases).
- The β_2 determines the stability of bifurcating periodic solutions: if $\beta_2 < 0$ ($\beta_2 > 0$), the periodic solution is asymptotically stable (unstable) in this central manifold.

Proof. Initially, the continuous real-valued function space is defined as $C = C([-1,0],\mathbb{R}^5)$ and convert system (4) to:

$$\dot{u}_1(t) = x(t) - x^*, \quad \dot{u}_2(t) = y(t) - y^*, \quad \dot{u}_3(t) = z(t) - z^*, \quad \dot{u}_4(t) = w(t) - w^*$$

Let $\tau = \tau_{10} + \mu$ where τ is defined by eq. (8). The general function differential equation can be obtained in the following form:

$$\dot{u}(t) = L_\mu(u_t) + F(\mu, u_t) \tag{10}$$

Then:

$$L_\mu(\phi) = (\tau_{10} + \mu)B\begin{pmatrix}\phi_1(0)\\ \phi_2(0)\\ \phi_3(0)\\ \phi_4(0)\end{pmatrix} + (\tau_{10} + \mu)C\begin{pmatrix}\phi_1(-1)\\ \phi_2(-1)\\ \phi_3(-1)\\ \phi_4(-1)\end{pmatrix}$$

and

$$F(\mu,\phi) = (\tau_{10} + \mu)\begin{pmatrix}(b - 3cx_*)\phi_1^2(0) - c\phi_1^3(0)\\ -f\phi_1^2(0)\\ 0\\ 0\end{pmatrix}$$

where

$$B = \begin{pmatrix}2bx_* - 3cx_*^2 & a & -d & 0\\ -2fx_* & 0 & 0 & 0\\ 0 & 0 & -\mu & 0\\ 0 & 0 & 0 & -vk\end{pmatrix}, \quad C = \begin{pmatrix}0 & 0 & 0 & 0\\ 0 & 0 & 0 & -g\\ 0 & 0 & 0 & 0\\ 0 & 0 & 0 & 0\end{pmatrix}$$

By the Riesz representation *Theorem*, there exists a 4×4 matrix function with bounded variables $\eta(\theta, \mu)$, $\theta \in [-1, 0]$ such that:

$$L_\mu\phi = \int_{-1}^{0} \mathrm{d}\eta(\theta,\mu)\phi(\theta), \quad \text{for} \quad \phi \in C([-1,0],\mathbb{R}^4)$$

In fact, we can choose:

$$\eta(\theta,\mu)=(\tau_{10}+\mu)B\delta(\theta)+(\tau_{10}+\mu)(C)\delta(\theta+1) \tag{11}$$

where δ is Dirac function.

For $\phi = C([-1, 0], R_4)$, define:

$$A(\mu)\phi(\theta)=\begin{cases}\dfrac{\mathrm{d}\phi(\theta)}{\mathrm{d}\theta} & \theta\in[-1,0)\\ \displaystyle\int_{-1}^{0}\mathrm{d}\eta(\theta,\mu)\phi(\theta) & \theta=0\end{cases} \tag{12}$$

and

$$R(\mu)\phi(\theta)=\begin{cases}0 & \theta\in[-1,0)\\ F(\mu,\phi) & \theta=0\end{cases} \tag{13}$$

Then the system (1) is equivalent to $\dot{x}_t = A(\mu)x_t + R(\mu)x_t$, where $x_t(\theta) = x(t+\theta)$, $\theta\in[-1,0]$.

For $\psi = C([0,1],(R^4)^*)$, define:

$$A^*(\mu)\psi(s)=\begin{cases}-\dfrac{\mathrm{d}\psi(s)}{\mathrm{d}s} & s\in(0,1]\\ \displaystyle\int_{-1}^{0}\mathrm{d}\eta(t,0)\psi(-t) & s=0\end{cases} \tag{14}$$

and a bilinear inner product:

$$\langle\psi(s),\phi(\theta)\rangle=\bar{\psi}(0)\phi(0)-\int_{-1}^{0}\int_{\xi=0}^{\theta}\bar{\psi}(\xi-\theta)\mathrm{d}\eta(\theta)\phi(\xi)\mathrm{d}\xi \tag{15}$$

where $\eta(\theta)=\eta(\theta,0)$, $A(0)$ and $A^*(0)$ are adjoint operators. We assume $\pm i\omega_0\tau_{10}$ are the eigenvalues of $A(0)$, then they are also the eigenvalues of $A^*(0)$. Let $q(\theta)$ be the eigenvectors of $A(0)$ corresponding to eigenvalue $+i\omega_0\tau_{10}$, and $q^*(0)$ be the eigenvectors of $A^*(0)$ corresponding to eigenvalue $-i\omega_0\tau_{10}$. Then $A(0)q(\theta)=i\omega_0\tau_{10}q(\theta)$, $A^*(0)q^*(\theta)=-i\omega_0\tau_{10}q^*(\theta)$.

Let $q(\theta)=(1,v_1,v_2,v_3)^T\mathrm{e}^{i\omega_0\tau_{10}\theta}$ and $q^*(\theta)=P(1,v_1^*,v_2^*,v_3^*)^T\mathrm{e}^{i\omega_0^*\tau_{10}\theta}$. Further calculations can be obtained:

$$v_1=\frac{-(2bx_*-3cx_*^2-i\omega_0)(\mu+i\omega_0)+g\mathrm{e}^{-i\omega_0\tau_{10}}}{\mu+i\omega_0},\quad v_2=\frac{-g\mathrm{e}^{-i\omega_0\tau_{10}}}{\mu+i\omega_0}$$

$$v_3=\frac{(2bx_*-3cx_*^2-i\omega_0)(\mu+i\omega_0)+g\mathrm{e}^{-i\omega_0\tau_{10}}}{(vk+i\omega_0)(\mu+i\omega_0)}$$

and

$$v_1^*=\frac{(2bx_*-3cx_*^2+i\omega_0)(i\omega_0-\mu)+g\mathrm{e}^{-i\omega_0\tau_{10}}}{2fx_*(i\omega_0-\mu)},\quad v_2^*=\frac{d}{i\omega_0-\mu}$$

$$v_3^*=\frac{(2bx_*-3cx_*^2+i\omega_0)(i\omega_0-\mu)(i\omega_0+vk)-g\mathrm{e}^{-i\omega_0\tau_{10}}(i\omega_0+vk)}{2fgx_*(i\omega_0-\mu)}$$

By using the same notions as in [9], since:

$$\left\langle q^*(s), q(\theta)\right\rangle = \bar{q}^*(0)q(0) - \int_{-1}^{0}\int_{\xi=0}^{\theta} \bar{q}^*(\xi-\theta)\mathrm{d}\eta(\theta)q(\xi)\mathrm{d}\xi$$

$$= \bar{P}(1,\bar{v}_1^*,\bar{v}_2^*,\bar{v}_3^*)(1,v_1,v_2,v_3)^T - \int_{-1}^{0}\int_{\xi=0}^{\theta} \bar{P}(1,\bar{v}_1^*,\bar{v}_2^*,\bar{v}_3^*)\mathrm{e}^{-i\omega_0\tau_{10}(\xi-\theta)}\mathrm{d}\eta(\theta)(1,v_1,v_2,v_3)^T\mathrm{e}^{i\omega_0\tau_{10}\xi}\mathrm{d}\xi$$

$$= \bar{P}\left\{1 + v_1\bar{v}_1^* + v_2\bar{v}_2^* + v_3\bar{v}_3^* + \bar{v}_2^*\mu s\tau_{10}\mathrm{e}^{-i\omega_0\tau_{10}}\right\}$$

we may choose:

$$P = \frac{1}{1 + \bar{v}_1 v_1^* + \bar{v}_2 v_2^* + \bar{v}_3 v_3^* + v_2^* g\tau_{10}\mathrm{e}^{i\omega_0\tau_{10}}} \tag{16}$$

$$\bar{P} = \frac{1}{1 + v_1\bar{v}_1^* + v_2\bar{v}_2^* + v_3\bar{v}_3^* + \bar{v}_2^* g\tau_{10}\mathrm{e}^{-i\omega_0\tau_{10}}} \tag{17}$$

which assure that $\left\langle q^*(s), q(\theta)\right\rangle = 1$ and $\left\langle q^*(s), \bar{q}(\theta)\right\rangle = 1$.

By using Hassard *et al.*'s judgment mark, see in [9], we compute the co-ordinates of the center manifold C_0 at $\mu = 0$, and have:

$$W(t,\theta) = W[z(t),\bar{z}(t)] = W_{20}(\theta)\frac{z^2}{2} + W_{11}(\theta)z\bar{z} + W_{02}(\theta)\frac{\bar{z}^2}{2} + \ldots \tag{18}$$

$$g(z,\bar{z}) = g_{20}\frac{z^2}{2} + g_{11}z\bar{z} + g_{02}\frac{\bar{z}^2}{2} + \ldots \tag{19}$$

where z and $\bar{z}$ are local co-ordinates for center manifold C_0 in the direction of q^* and $\bar{q}^*$.

Comparing the coefficients with the eq. (19), we obtain:

$$g_{20} = g_{11} = g_{02} = 2\bar{P}\tau_{10}(b - 3cx_* - f\bar{v}_1^*)$$

$$g_{21} = 2\bar{P}\tau_{10}[(b - 3cx_*)(W_{20}^{(1)} + 2W_{11}^{(1)}) - 3c - f(W_{20}^{(1)} + 2W_{11}^{(1)})\bar{v}_1^*]$$

where

$$W_{20}(\theta) = \frac{ig_{20}}{\omega_0\tau_{10}}q(0)\mathrm{e}^{i\omega_0\tau_{10}\theta} + \frac{i\bar{g}_{02}}{3\omega_0\tau_{10}}\bar{q}(0)\mathrm{e}^{-i\omega_0\tau_{10}\theta} + E_1\mathrm{e}^{2i\omega_0\tau_{10}\theta}$$

$$W_{11}(\theta) = -\frac{ig_{11}}{\omega_0\tau_{10}}q(0)\mathrm{e}^{i\omega_0\tau_{10}\theta} + \frac{i\bar{g}_{11}}{\omega_0\tau_{10}}\bar{q}(0)\mathrm{e}^{-i\omega_0\tau_{10}\theta} + E_2$$

and

$$E_1 = \begin{pmatrix} 2i\omega_0\tau_{10} - (2bx_* - 3cx_*^2) & -a & d & 0 \\ 2fx_* & 2i\omega_0\tau_{10} + \mathrm{e}^{-2i\omega_0\tau_2^*} & 0 & g\mathrm{e}^{-2i\omega_0\tau_{10}^*} \\ -\mu s & 0 & 2i\omega_0\tau_{10} + \mu & 0 \\ 0 & -vr & 0 & 2i\omega_0\tau_{10} + vk \end{pmatrix}^{-1} \begin{pmatrix} 2(b - 3cx_*) \\ -2f\bar{v}_1^* \\ 0 \\ 0 \end{pmatrix}$$

$$E_2 = -\begin{pmatrix} 2bx_* - 3cx_*^2 & a & -d & 0 \\ -2fx_* & -1 & 0 & -g \\ \mu s & 0 & -\mu & 0 \\ 0 & vr & 0 & -vk \end{pmatrix}^{-1} \begin{pmatrix} 2(b - 3cx_*) \\ -2f\bar{v}_1^* \\ 0 \\ 0 \end{pmatrix}$$

Thus, we can compute the following values:

$$c_1(0) = \frac{i}{\omega_0\tau_{10}}\left(g_{11}g_{20} - 2|g_{11}|^2 - \frac{|g_{02}|^2}{3}\right) + \frac{g_{21}}{2}, \quad \mu_2 = -\frac{\mathrm{Re}[c_1(0)]}{\mathrm{Re}[\lambda_0'(\tau_{10})]}$$
$$\beta_2 = 2\,\mathrm{Re}[c_1(0)], \quad T_2 = -\frac{\mathrm{Im}[c_1(0)] + \mu_2\,\mathrm{Im}[\lambda_0'(\tau_{10})]}{\omega_0\tau_{10}} \tag{20}$$

In summary, we can get the following conclusions about the direction of Hopf bifurcation and the stability of periodic solutions.

Chaos-mediated mixed-mode oscillations

Every time we make a minor change in the system parameters, the dynamics of the system will change in some way. In the Hindmarsh-Rose neuronal oscillator experiment, a change in one parameter will often lead to a subsequent change in the other parameters. Thus, it is possible to study the effect of multiple parameters on the system's dynamical behavior under simultaneous variation. Additionally, the dynamical behavior of the system becomes richer with the addition of time delay. In this section, the parameters I_{DC} and v will be chosen to study the variation of the periodic cluster discharge behavior of the system at different time delays.

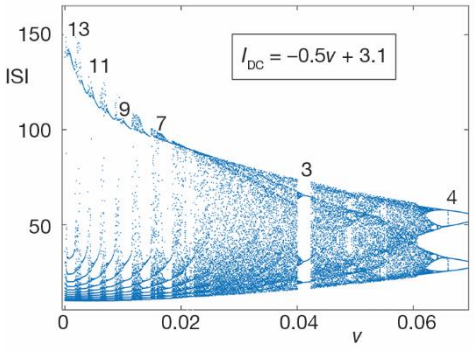

Figure 1. Bifurcation diagram of the system (1) *vs.* the parameter *v*

When varying the parameter v with stimulus current I_{DC}, where I_{DC} is –0.5v + 3.1, a bifurcation diagram about parameter v can be obtained as in fig. 1. It can be observed that as the parameter v gradually decreases, the periodic cluster discharge increases from period-4 in succession, accompanied by the phenomenon of doubled-cycle bifurcation. It can be found that the conversion process of every two-cycle cluster discharge is accompanied by a chaotic phenomenon, which is called chaos-mediated mixed-mode oscillations.

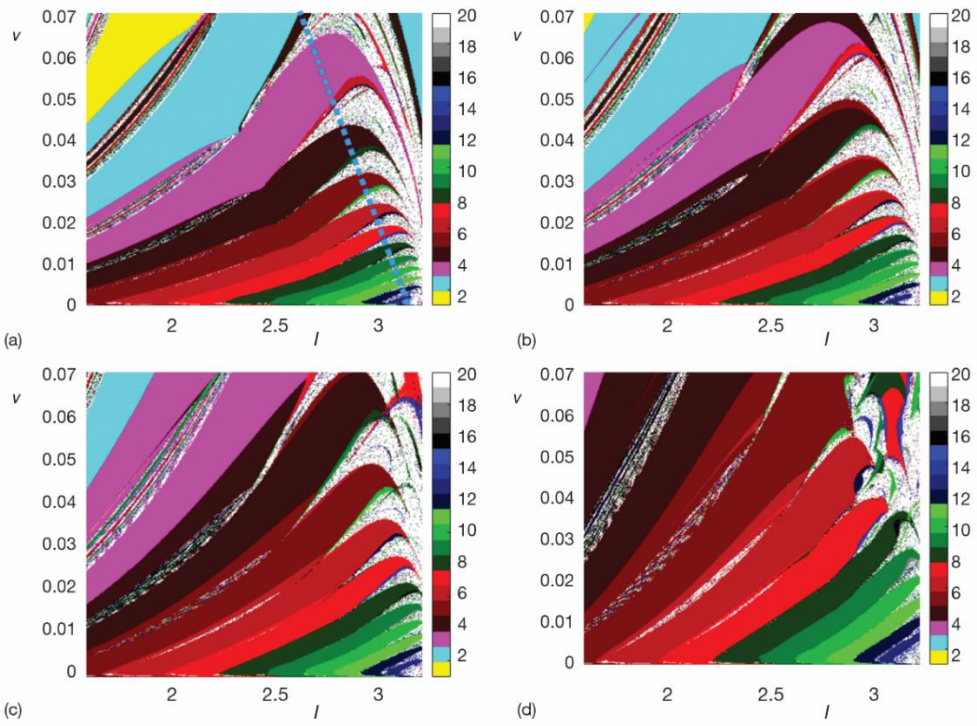

Figure 2. Periodic bifurcation diagram with chaos; (a) $\tau = 0.5$, (b) $\tau = 1$, (c) $\tau = 5$, and (d) $\tau = 10$

A similar phenomenon is observed in the two-parameter bifurcation diagram. Keep I_{DC} be $-0.5v + 3.1$, when parameter v is variable, which is corresponding to the blue dotted line in fig. 2(a). It can be seen that when the parameter v is 0.07, the system is a period-4 cluster discharge. Similar to the phenomenon in fig. 1, as the parameter v decreases along the direction of the blue dashed line, the system (2) enters the chaotic phenomenon *via* period 4 and then evolves into the period 3 state, followed by the octave bifurcation and chaotic phenomenon. Afterwards, many typical nonlinear behaviors take place, involving period 4 motion, octave state, chaotic phenomenon and so on, and finally it stops at period-13.

In figs. 2(a)-2(d), the time delay increases sequentially. It can be found that spike discharges and period-2 cluster discharges gradually disappear, and high-period cluster discharges gradually occupy the main body. It can be seen that when the time hysteresis is large enough, the whole area will be occupied by high period and the chaotic phenomenon will disappear and become non-chaos-mediated mixed-mode oscillations.

Non-chaos-mediated mixed-mode oscillations

In the previous section, chaos-mediated mixed-mode oscillations was discussed, and this section will discuss the case where there is no chaos window. From fig. 3, it can be observed that as the stimulation current increases, the number of periodic cluster discharges increases sequentially ranging from period-4, period-5, period-6 to period-13. Further, a two-parameter plane with respect to the parameters, I, and, v, is constructed. As can be seen in fig. 4, as the time delay increases, the high-period cluster discharge behavior gradually disappears in the blue rectangular region.

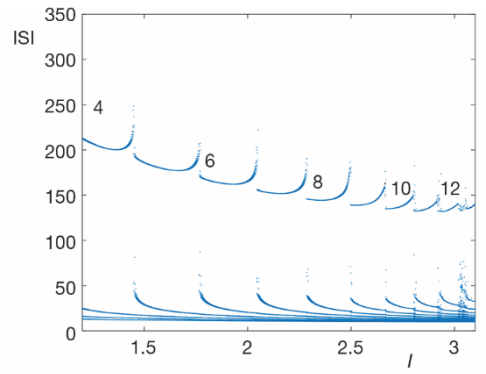

Figure 3. Bifurcation diagram of the system (1) *vs.* the parameter *I*

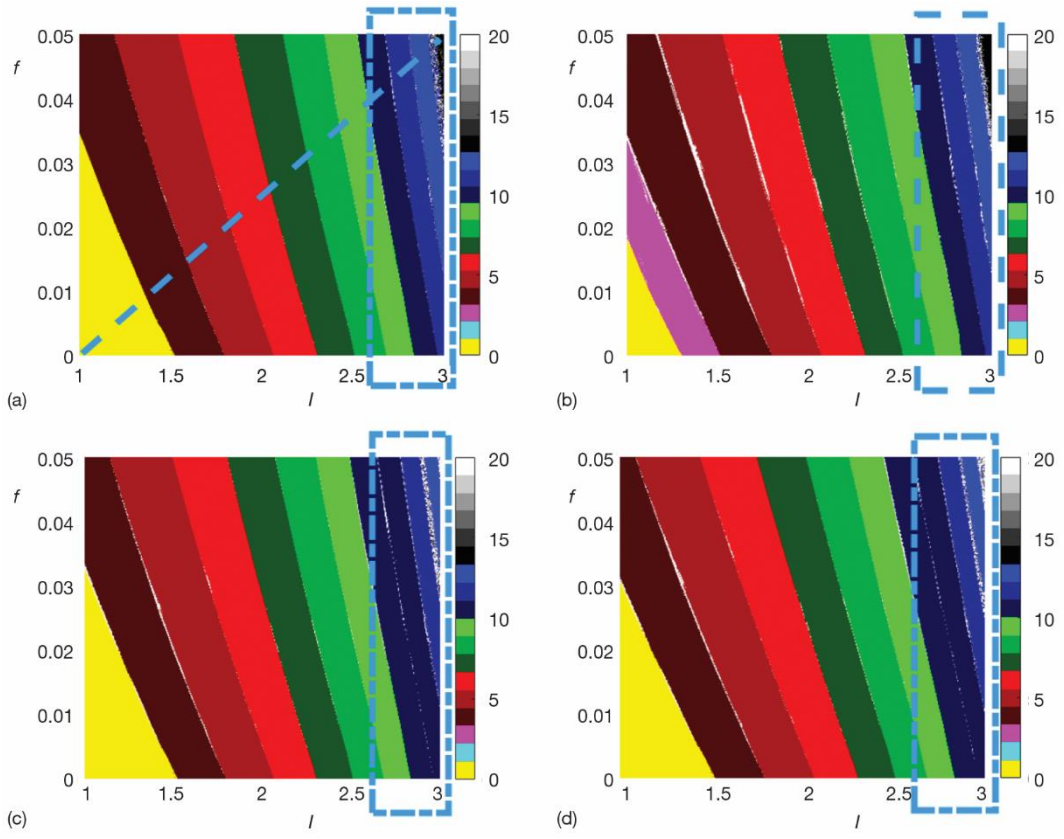

Figure 4. Periodic bifurcation diagram with chaos; (a) $\tau = 0.5$, (b) $\tau = 5$, (c) $\tau = 10$, and (d) $\tau = 15$

Conclusions

In this paper, we focus on the extended Hindmarsh-Rose neuronal oscillator and analyze the effect of different parameters on the dynamical behavior of the extended Hindmarsh-Rose neuronal oscillator under the influence of time delay through single-parameter

and two-parameter bifurcation diagrams. The first gives a classical chaos-mediated mixed-mode oscillation in which the interval between different periodic oscillations is always separated by a chaotic window in which the lower-period low-discharge mode gradually disappears and the higher-period generation mode dominates as the time delay increases. In addition, a non-chaotic-mediated mixed-mode oscillation phase is proposed in which a chaotic window does not exist, after which the motion states related to the system experiences period-5, period-6 and period-7 till the end of period-14. As the time delay increases, the resting states' region expands and the high-period discharge pattern then moves backward. This paves the way for future studies to understand abnormal neuronal discharges and control discharge patterns.

Acknowledgment

This work was supported by the National Natural Science Foundation (No. 61863022, 11962012), and the Innovation and Entrepreneurship of Lanzhou City (No. 2018-RC-87).

References

[1] Wu, K., *et al.*, Bifurcation Study of Neuron Firing Activity of the Modified Hindmarsh-Rose Model, *Neural Computing & Applications*, *27* (2016), 3, pp. 739-747
[2] Rech, P. C., The Dynamics of a Symmetric Coupling of Three Modified Quadratic Maps, *Chinese Physics B*, *22* (2013), 8, 080202
[3] Junges, L., Gallas, J. A. C., Stability Diagrams for Continuous Wide-Range Control of Two Mutually Delay-Coupled Semiconductor Lasers, *New Journal of Physics*, *17* (2015), May, 053038
[4] Golomb, D., Mechanism and Function of Mixed-Mode Oscillations in Vibrissa Motoneurons, *PLoS One*, *9* (2014), 10, e109205
[5] Bi, W., *et al.*, Oscillatory Electro-Oxidation of Thiosulfate on Gold, *Electrochimica Acta*, *133* (2014), Jun., pp. 308-315
[6] Tang, K., *et al.*, Electrical Activity in a Time-Delay Four-Variable Neuron Model under Electromagnetic Induction. *Frontiers in Computational Neuroence*, *21* (2017), 11, 105
[7] Zhang, Z., *et al.*, Stability and Hopf Bifurcation Analysis of an SVEIR Epidemic Model with Vaccination and Multiple Time Delays, *Chaos, Solitons and Fractals*, *131* (2020), Feb., 109483
[8] Ngouonkadi, E. B. M., *et al.*, Bifurcations and Multistability in the Extended Hindmarsh-Rose Neuronal Oscillator, *Chaos, Solitons & Fractals*, *85* (2016), Apr., pp. 151-163
[9] Al-Hussein, A. B. A., *et al.*, Hopf Bifurcation and Chaos in Time-Delay Model of Glucose-Insulin Regulatory System, *Chaos Solitons & Fractals*, *137* (2020), Aug., 109845
[10] He, C. H., *et al.*, Hybrid Rayleigh-Van Der Pol-Duffing Oscillator: Stability Analysis and Controller, *Journal of Low Frequency Noise Vibration and Active Control*, *41* (2021), 1, pp. 244-268
[11] He, J. H., *et al.*, Dynamic Pull-in for Micro-Electromechanical Device with a current-Carrying Conductor, *Journal of Low Frequency Noise Vibration and Active Control*, *40* (2021), 2, pp. 1059-1066
[12] He, J.-H., *et al.*, Periodic Property and Instability of a Rotating Pendulum System, *Axioms*, *10* (2021), 191
[13] Feng, G. Q., He's Frequency Formula to Fractal Undamped Duffing Equation, *Journal of Low Frequency Noise Vibration and Active Control*, *40* (2021), 4, 1671-1676
[14] He, C. H., *et al.*, Low Frequency Property of a Fractal Vibration Model for a Concrete Beam, *Fractals*, *29* (2021), 5, 150117
[15] He, J. H., *et al.*, Nonlinear Instability of Two Streaming-Superposed Magnetic Reiner-Rivlin Fluids by He-Laplace Method, *Journal of Electroanalytical Chemistry*, *895* (2021), Aug., 115388
[16] Wang, K. L., He, C. H., A Remark on Wang's Fractal Variational Principle, *Fractals*, *27* (2019), 8, 1950134
[17] Wang, K. L., *et al.*, Physical Insight of Local Fractional Calculus and Its Application to Fractional KdV-Burgers-Kuramoto Equation, *Fractals*, *27* (2019), 7, 1950122

[18] Ismail, G. M., *et al.*, Analytical Study of the Vibrating Double-Sided Quintic Non-linear Nano-Torsional Actuator Using Higher-Order Hamiltonian Approach, *Journal of Low Frequency Noise Vibration and Active Control, 41* (2021), 1, pp. 269-277
[19] He, J. H., *et al.*, Variational Approach to Fractal Solitary Waves, *Fractals*, *29* (2021), 7, 2150199
[20] Wang, K. J., Generalized Variational Principle and Periodic Wave Solution to the Modified Equal Width-Burgers Equation in Non-linear Dispersion Media, *Physics Letters A*, *419* (2021), Dec., 127723
[21] Li, X. X., He, C. H., Homotopy Perturbation Method Coupled with the Enhanced Perturbation Method, *Journal of Low Frequency Noise Vibration and Active Control, 38* (2019), 3-4, pp. 1399-1403
[22] He, J.-H., *et al.*, Homotopy Perturbation Method for the Fractal Toda Oscillator, *Fractal Fract., 5* (2021), 93, 5030093
[23] Han, C., *et al.*, Numerical Solutions of Space Fractional Variable-Coefficient KdV-Modified KdV Equation by Fourier Spectral Method, *Fractals*, *29* (2021), 8, 21502467-1602
[24] Tian, Y., Liu, J., Direct Algebraic Method for Solving Fractional Fokas Equation, *Thermal Science*, *25* (2021), 3, pp. 2235-2244
[25] He, Y., Li, H. B., A Novel Numerical Method for Heat Equation, *Thermal Science*, *20* (2016), 3, pp. 1018-1021

Paper submitted: November 20, 2020
Paper revised: October 1, 2021
Paper accepted: October 1, 2021